Fuel 279 (2020) 118372

Contents lists available at ScienceDirect

Fuel

journal homepage: www.elsevier.com/locate/fuel

Full Length Article

Highly active Pd catalysts supported on surface-modified cobalt-nickel mixed oxides for low temperature oxidation of lean methane

Cunshuo Li, Wenzhi Li*, Kun Chen, Ajibola T. Ogunbiyi, Zean Zhou, Qiuyan Duan, Fengyang Xue

Laboratory of Basic Research in Biomass Conversion and Utilization, Department of Thermal Science and Energy Engineering, University of Science and Technology of China, Hefei 230026, China

ARTICLE INFO

Keywords:
Palladium
Cobalt-nickel mixed oxides
Surface modification
Synergistic interaction
Lean methane combustion

ABSTRACT

A highly active palladium catalyst supported on SiO_2-modified cobalt-nickel mixed oxide (denoted as 0.5Pd/M-Co_1Ni_4) was prepared and used for lean methane combustion. It was found that such a surface modification strategy enhanced the synergistic interaction between deposited palladium phase and reactive cobalt-nickel oxide, leading to substantial improvement in performance towards methane combustion. Over 0.5Pd/M-Co_1Ni_4, 90% methane conversion was realized at 323°C and a space velocity of 60,000 $mL g^{-1} h^{-1}$, which is 62 °C lower than that required for its untreated counterpart, 0.5Pd/Co_1Ni_4. The results of XRD, TEM, transmission FTIR and XPS demonstrated that the introduced SiO_2, which was presented as an amorphous phase covering the carrier surface, could effectively tune the electronic structure of both Co_1Ni_4 support and palladium entities. More importantly, H_2-TPR and O_2-TPD results of 0.5Pd/M-Co_1Ni_4 revealed that the presence of SiO_2 could enhance the low-temperature redox capability and increase the supply of oxygen species during the reaction process. We believe that the combination of PdO_x ($1 < x < 2$) phase and modified Co_1Ni_4 oxide with low Co^{3+}/Co^{2+} ratio was responsible for such an excellent performance of 0.5Pd/M-Co_1Ni_4. This work provides a feasible method for the design of efficient CCM catalysts with reduced palladium content by maximizing the palladium species and reactive host materials.

1. Introduction

With increasingly severe emission regulations, natural gas (> 95% methane, CH_4) has been gradually considered as an alternative to petrol-based fuel for automotive applications [1]. Under this circumstance, natural gas vehicles (NGVs) which exhibit significant environmental advantages because of lower emissions of solid particles [2] and carbon dioxide [3], have gained popularity in many countries and their number is anticipated to grow over time [4]. However, the advantages of NGVs are partially counteracted by the release of unburned lean methane, which possesses more than 20 times higher global warming potential than CO_2 [5]. To date, catalytic combustion of methane (CCM) has become a competitive technology to remove this environmental pollutant owing to its high combustion efficiency and little emissions of other by-products, such as NO_x and CO [2].

The first priority in CCM is to develop catalysts that show sufficient activity at low temperatures, and over the past decades, a great deal of research has been done in this regard. Among the available catalysts, supported palladium catalysts are most active owing to their capability to initiate methane molecules at temperatures below 400°C. Pd-based catalysts supported on CeO_2 are well-studied [6–8], and other metal oxides including Al_2O_3 [9,10], SnO_2 [11,12], SiO_2 [13,14] and ZrO_2 [15,16] have also served as host materials for active palladium phases, as seen in literature. Meanwhile, catalysts made of transition metal (especially Co, Ni, Cu, Cr and Mn) oxides and derived mixed oxides (such as manganese-nickel [17], cobalt-chromium [18], cobalt-nickel [19,20], manganese-cobalt [21] and copper-manganese [22] based mixed oxides) have also been developed and recognized as appealing substitutes for noble metals towards methane combustion. Generally speaking, due to higher oxygen mobility, mixed oxides show better catalytic capabilities than single transition metal oxides, though their activities per site are still lower than those of Pd-based catalysts.

Irrespective of the excellent activities of palladium-based catalysts, their rarity and high price limit their industrial applications. Consequently, current research has mainly focused on pursuing effective CCM catalysts with reduced Pd content via maximizing the active palladium species. Towards this goal, Cragnello et al. developed a surface modification strategy using organ-silane as surfactant in 2012. They claimed that the hydrophobic Al_2O_3 support improved the dispersion of Pd@CeO_2 subunits, and the enhanced Pd-CeO_2 interaction

* Corresponding author.
E-mail address: liwenzhi@ustc.edu.cn (W. Li).

https://doi.org/10.1016/j.fuel.2020.118372
Received 26 April 2020; Received in revised form 3 June 2020; Accepted 9 June 2020
Available online 07 July 2020
0016-2361/

was key factor responsible for the exceptional performance of Pd@CeO_2/H-Al_2O_3 catalyst [23]. Inspired by this seminal effort, we recently demonstrated that the synthesis of atomically dispersed palladium catalysts could be achieved via constructing a spatial structure between active phase and surface-modified support; the utmost utilization of palladium entities enabled the 0.23 wt%Pd/SiO_2-ZrO_2 catalyst to remove all lean methane at only 400℃ [24]. On the other hand, the catalytic performance of Pd-containing catalysts also depends on the properties of their supports which affect the Pd-support interaction [25]. Therefore, adopting intrinsically active materials as carriers for palladium represents another promising option for lowering the amount of noble metal while guaranteeing the low-temperature performance of CCM catalysts. Pd-containing catalysts supported on reactive Co_3O_4 spinel (3% Pd/Co_3O_4) [26], Co_3O_4 nanorods (PdO/Co_3O_4 nanorods) [27] and three-dimensionally ordered mesoporous (3DOM) Co_3O_4 (2.94$Au_{0.50}$Pd/meso-Co_3O_4) [28] have been reported by researchers. In these three systems, the synergistic interaction between palladium and Co_3O_4 provided excellent low-temperature activities towards methane combustion, but the contents of noble metals of these three samples were somehow high. With this consideration, our reported Co_1Ni_4 (with a Co/Ni ratio of 1:4) catalyst [19], which displayed better light-off performance than pure Co_3O_4 at low temperature, seems to be a more promising host material for further reducing the loading amount of noble metals. Overall, the reviewed literature allowed one to expect that a combination of Co_1Ni_4 oxides and palladium species might make the best use of these two reactive materials, and a surface modification strategy may further tune their synergistic interaction and improve the low-temperature activity of this catalyst system.

Thus, we herein report the fabrication of highly active palladium catalysts supported on SiO_2-modified cobalt-nickel mixed oxides and their application for lean methane combustion. The Co_1Ni_4 oxides were adopted as supports, which had high hydrothermal stability and reactivity under CH_4-lean reaction environment. The effect of surface modification of Co_1Ni_4 support on the catalytic performance for CH_4 combustion was then evaluated. Subsequently, several characterization techniques were employed to study the physicochemical properties determining the outstanding performance of 0.5Pd/M-Co_1Ni_4.

2. Experimental

2.1. Preparation of catalysts

The cobalt-nickel oxides with specific Co/Ni ratio of 1:4 were prepared by co-precipitation method [19] using cobalt nitrate ($Co(NO_3)_2$) and nickel nitrate ($Ni(NO_3)_2$) as precursors and ammonium hydroxide ($NH_3{\cdot}H_2O$) as a precipitator.

The surface modification of Co_1Ni_4 supports was carried out using Cargnello's method with slight changes [23]. Typically, 5 g of support powder and 2.75 mL of triethoxy-n-octysilane (TEOOS, 97%) were first dispersed in 100 mL toluene by sonication for 20 min. Under vigorous stirring, the mixture was then refluxed at 110℃ for 3 h, after which the oxide powder was purified by centrifugation (6000 rpm, 3 min) and subsequently washed with toluene three times. Finally, the hydrophobic support was obtained by drying under vacuum and stored as host material for preparing supported palladium catalysts.

Supported palladium catalysts were synthesized by impregnation method. A typical preparation of catalyst with desired palladium content of 0.5 wt% was carried out according to the following procedure. 5.3 mL of palladium acetate solution (2 mg/mL, dissolved in toluene) was stirred with 1 g of hydrophobic support for 10 min, then the mixture was sonicated for another 20 min and dried at 70℃ under −0.09 MPa vacuum overnight. The sample was finally calcined at 500℃ for 3 h using a ramp of 5 ℃min^{-1}.

In this study, the hydrophobic Co_1Ni_4 oxide (the refluxed support without calcination) is denoted as H-Co_1Ni_4. After the calcination at 500℃, the silanes bound on the surface of H-Co_1Ni_4 decomposed to SiO_2 and, therefore, this modified support and the corresponding supported Pd catalyst are designated as M-Co_1Ni_4 and 0.5Pd/M-Co_1Ni_4, respectively. Likewise, palladium catalysts supported on untreated Co_1Ni_4 are tagged 0.5Pd/Co_1Ni_4. For comparison, certain amounts of H-Co_1Ni_4 and Co_1Ni_4 supports were also calcined at 500℃ for 3 h before performance evaluation and characterization.

2.2. Catalyst characterization and activity measurement

The physicochemical properties of representative samples were characterized by inductively coupled plasma-atomic emission spectrometer (ICP-AES), N_2-physisorption (Brunauer-Emmett-Teller, BET), X-ray diffraction (XRD), field-emission transmission electron microscope (FETEM), fourier transform infrared (FTIR) spectroscopy, X-ray photoelectron spectroscopy (XPS), hydrogen-temperature programmed reduction (H_2-TPR) and oxygen temperature programmed desorption (O_2-TPD). Details on the characterization procedures were described in Supplementary material. Lean methane combustion (1.0 vol% CH_4, 60,000 mL$g^{-1}h^{-1}$) over the obtained catalysts was also conducted according to the method provided in Supplementary material.

3. Results and discussion

3.1. Catalysts characterization: ICP-AES and BET

The actual contents of palladium in 0.5Pd/Co_1Ni_4 (0.48 wt%) and 0.5Pd/M-Co_1Ni_4 (0.45 wt%) were determined by ICP-AES, which are close to their nominal percentages. Regretfully, the chemisorption technique employed to determine the Pd dispersion over irreducible supports (SiO_2, Al_2O_3) cannot be used in our catalyst system, since H_2 or CO chemisorbs on both Co_1Ni_4 supports and PdO_x phases [26]. Table 1 lists the BET surface areas of samples estimated by nitrogen adsorption–desorption analysis. M-Co_1Ni_4 and 0.5Pd/M-Co_1Ni_4 show higher BET values than Co_1Ni_4 and 0.5Pd/Co_1Ni_4, proving that the surface modification of support increased the surface areas of samples. Nevertheless, there is no definite correlation between the BET value and light-off performance of these samples, which means that heat and mass transfer limitations might not have existed in our reaction system.

3.2. Crystal structure and morphology

The XRD patterns of Co_1Ni_4, M-Co_1Ni_4, 0.5Pd/Co_1Ni_4 and 0.5Pd/M-Co_1Ni_4 are displayed in Fig. 1. As can be seen, a combined phase of NiO and $NiCo_2O_4$ existed in all the four catalysts, while the modification of

Table 1
Specific surface areas and surface composition of selected samples.

Catalyst	S_{BET}[a] [m^2g^{-1}]	Co^{3+}/Co^{2+} [b] [mol/mol]	O_{ads}/O_{latt} [b] [mol/mol]	Pd^{4+}/Pd^{2+} [b] [mol/mol]	Content of Si [b] [wt%]
Co_1Ni_4	18.44	0.73	0.41	—	—
M-Co_1Ni_4	19.10	0.75	0.37	—	5.29
0.5Pd/Co_1Ni_4	18.95	0.70	0.40	0.23	—
0.5Pd/M-Co_1Ni_4	23.63	0.62	0.39	0.59	5.16

a. BET method. b. Determined by XPS.

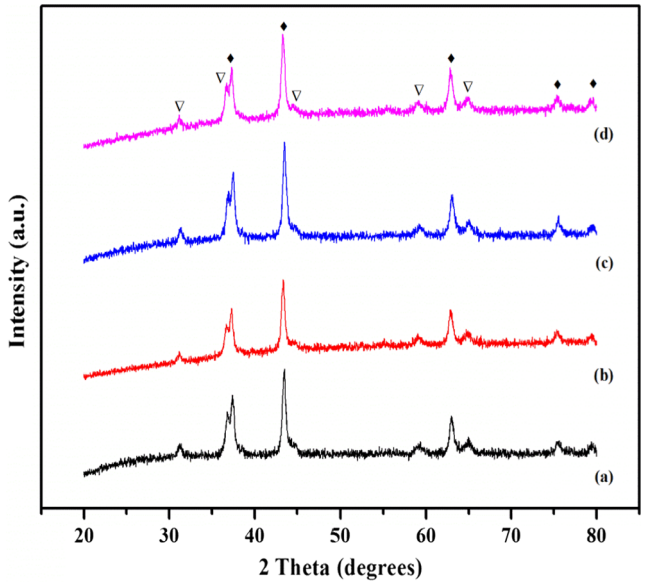

Fig. 1. XRD patterns of (a) Co_1Ni_4, (b) M-Co_1Ni_4, (c) 0.5Pd/Co_1Ni_4 and (d) 0.5Pd/M-Co_1Ni_4. Crystalline phases detected: (♦) NiO, (▽) $NiCo_2O_4$.

support and the deposition of palladium species did not alter the crystalline structure of these samples. Specifically, the Bragg diffraction peaks of 2θ values of 31.2°, 36.7°, 44.6°, 59.1° and 65.0° are ascribed to the Fd3m space group of $NiCo_2O_4$ spinel phase (JCPDS PDF #47-1049), while the peaks at 37.2°, 43.3°, 62.9°, 75.4° and 79.4° can be assigned to the NiO Phase (JCPDS PDF #73-1072). This composition is reasonable considering the realistic Co/Ni ratio, since only NiO can be formed once the amount of Ni^{2+} exceeds the capacity of spinel octahedral sites. [29,30] In addition, no peak associated with metallic Pd (2θ = 40°, 46°) or PdO (2θ = 34°, 42°) [3,31] is detected in 0.5Pd/Co_1Ni_4 and 0.5Pd/M-Co_1Ni_4. This is an indication that the palladium crystallites were uniformly distributed throughout these two samples and/or are smaller than 3 nm [32]. Meanwhile, although the existence of SiO_2 is evidenced by the FTIR and XPS spectra shown in Fig. 3 and Fig. 4E, no standard peaks of SiO_2 phase can be observed in M-Co_1Ni_4 and 0.5Pd/M-Co_1Ni_4 samples. This is probably because either the SiO_2 covering the surface of support is exclusively amorphous or its crystallites are smaller than the resolution of XRD technique.

The morphology and size of 0.5Pd/Co_1Ni_4 and 0.5Pd/M-Co_1Ni_4 were investigated by TEM and HRTEM. As shown in Fig. 2a and Fig. 2b, Co_1Ni_4 mixed oxides take on irregular shapes with grain sizes in a wide range of 30–80 nm. Meanwhile, no palladium nanoparticles (NPs) could be imaged over the samples, suggesting that palladium species were presented as ultrafine crystallites in these two samples. Furthermore, HRTEM was also employed to understand the composition and the exposed lattice planes of 0.5Pd/Co_1Ni_4 and 0.5Pd/M-Co_1Ni_4. As shown in Fig. 2c, two kinds of interplanar distances of 0.243 nm and 0.470 nm can be clearly observed while Fig. 2d displays lattice fringe spaces of 0.239 nm and 0.240 nm. A spacing value of ~0.24 nm corresponds to the (2 2 2) plane of NiO [17], and that of ~ 0.47 nm is close to the *d* values of (1 1 1) lattice plane of spinel Co_3O_4 sample (about 0.46 nm) [28], which can be reasonably indexed to $NiCo_2O_4$ species considering the larger radius of Ni^{2+} (0.069 nm) [17] in comparison with that of Co^{3+} (0.055 nm) [18]. Such a mixed phase consisting of NiO and $NiCo_2O_4$ is also consistent with XRD results. Notably, on the surface of 0.5Pd/M-Co_1Ni_4, an amorphous (but not fully covered) phase with uneven thickness can be found simultaneously, probably because of the introduction of silicon species.

To prove this deduction, transmission FTIR spectra of pristine Co_1Ni_4 and hydrophobic Co_1Ni_4 oxide (H-Co_1Ni_4) were further collected and shown in Fig. 3. Based on published data, the weak absorption bands near 1664 cm^{-1} arise from H-O-H bending vibrations mode due to adsorption of water, and the features from 3000 to 3750 cm^{-1} are caused by hydroxyl species, while the vibration of Si-O bond and Ni-O gives bands at 1140 cm^{-1} [33] and 490 cm^{-1} [34,35], respectively. Considering that the hydrophobic Co_1Ni_4 powder had been rinsed abundantly and dried overnight before the FTIR measurement, the signal of unreacted TEOOS would be virtually negligible. Hence, the much stronger intensities of Si-O vibration band in H-Co_1Ni_4 can be associated with the attachment of long alkyl chains to the surface of Co_1Ni_4 support. Actually, the alkoxy groups of TEOOS were prone to hydrolysis during the reflux process at 110℃, but the alkyl chain was not [23]. As a result of the reaction between TEOOS and the support, the Co_1Ni_4 oxides were covered by alkyl chains and became hydrophobic, after which the alkyl chains evolved into SiO_2 modification layer during the 500℃-calcination eventually.

3.3. Chemical and electronic states

XPS spectra of Co 2p, Ni 2p, O 1s, Pd 3d and Si 2p are used to elucidate the surface composition of selected samples and local atomic environment of each element. By using deconvoluting method, the XPS spectra of Co 2p (Fig. 4A) could be fitted with Co $2p_{3/2}$ and Co $2p_{1/2}$ peaks at 779.8 eV and 795.7 eV in addition to two satellite peaks at 785.1 eV and 802.8 eV, respectively. The deconvoluted Co $2p_{3/2}$ peaks centered at lower binding energies (BEs) can be well indexed to Co^{3+} (779.8 eV) and Co^{2+} (781.6 eV) [30] while their relative percentages can be obtained by quantitative analysis based on their integral areas of corresponding peaks, as summarized in Table 1. It is obvious that upon loading palladium species, the Co^{3+}/Co^{2+} molar ratio of 0.5Pd/Co_1Ni_4 (0.70) and 0.5Pd/M-Co_1Ni_4 (0.62) decreased to much lower values in comparison with those of their supports. The drop in surface Co^{3+} concentration might be attributed to the transformation of palladium species discussed below, while the rise in Co^{2+} concentration is usually accompanied with increased concentration of oxygen vacancies in cobalt spinel structure [26,28]. In addition, there was also a good correlation between catalytic performance and Co^{3+}/Co^{2+} atomic ratio in the four samples, as reflected in the lowest Co^{3+}/Co^{2+} atomic ratio in our best-performing 0.5Pd/M-Co_1Ni_4, which illustrated that the oxidation state of Co is tightly related to the Pd-support interaction.

The multimodal Ni 2p spectra (Fig. 4B) of the catalysts are characterized by the Ni $2p_{1/2}$ and Ni $2p_{3/2}$ peaks together with two corresponding satellites with binding energies of about 7 eV higher. The Ni $2p_{3/2}$ lines are best fitted with doublet peaks at 856.2 and 854.3 eV, illustrating that the nickel components were mainly present as Ni^{2+} in these samples [17,19]. It is noteworthy that after the loading of palladium phases, the binding energies of 0.5Pd/Co_1Ni_4 and 0.5Pd/M-Co_1Ni_4 shifted towards the lower BE direction (especially in the latter sample), though the deposition of palladium did not alter the valency of nickel species.

The asymmetrical O 1s spectra shown in Fig. 4C display three peaks situated at binding energies of 529.8, 531.5 and 532.3 eV, respectively. As reported in literature, the peaks centered at lowest BE values (529.3–530.4 eV) are caused by lattice oxygen (O_{latt}, e.g., O^{2-}), while adsorbed oxygen species (O_{ads}, e.g., O_2^{2-}, O_2^- or O^-) give signals located at 530.8–531.5 eV. Components with BE values of 531.8–533.4 eV belong to the surface hydroxyl (O_{OH}) species and adsorbed water molecules [6,36]. On the basis of these assignments, one can deduce that all of the three oxygen components existed in each sample. The intensities of hydroxyl-related peaks in M-Co_1Ni_4 and 0.5Pd/M-Co_1Ni_4 are significantly stronger than those in Co_1Ni_4 and 0.5Pd/Co_1Ni_4, which might have come from Si-OH species because of the introduction of silicon species. In addition, it is generally accepted that the O_{ads}/O_{latt} ratio is a criterion to describe the proportion of active vacant oxygen on the catalyst surface [36]. However, one can propose that O_{ads}/O_{latt} ratio itself may not be an adequate index of enhanced reactivity due to the very close O_{ads}/O_{latt} values (see Table 1) in our

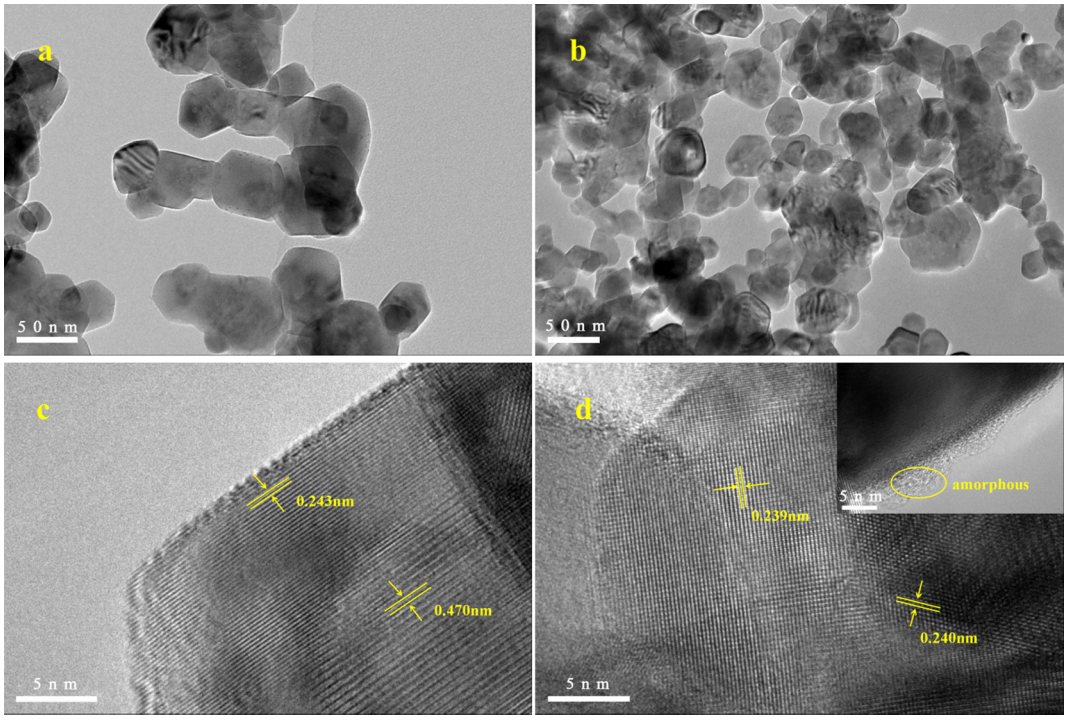

Fig. 2. TEM images of (a) 0.5Pd/Co_1Ni_4, (b) 0.5Pd/M-Co_1Ni_4 and HRTEM images of (c) 0.5Pd/Co_1Ni_4, (d) 0.5Pd/M-Co_1Ni_4.

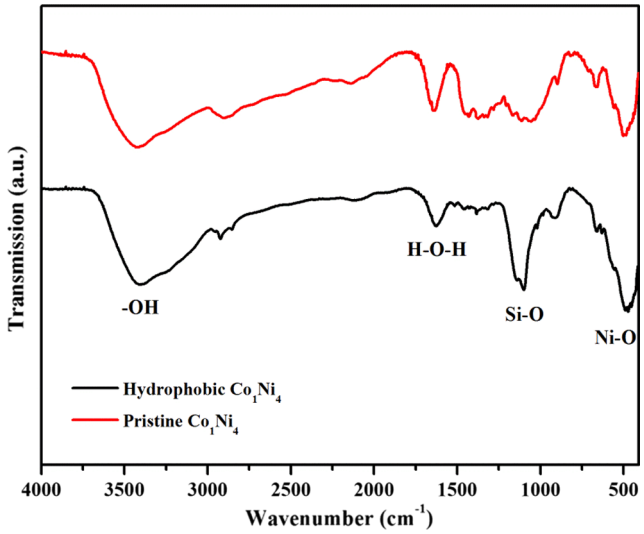

Fig. 3. Transmission FTIR spectra of pristine Co_1Ni_4 and hydrophobic Co_1Ni_4.

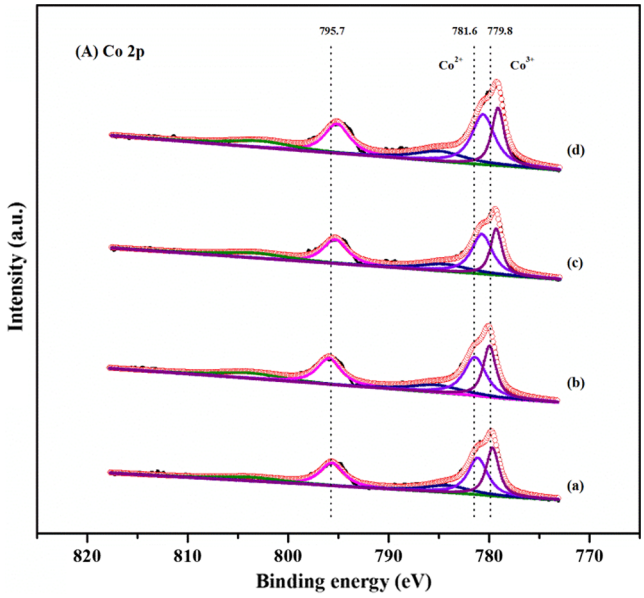

Fig. 4a. Co 2p XPS spectra of (a) Co_1Ni_4, (b) M-Co_1Ni_4, (c) 0.5Pd/Co_1Ni_4 and (d) 0.5Pd/M-Co_1Ni_4.

four samples. Taking into account that XPS tests were carried out at room temperature and ultrahigh vacuum, the results obtained from this ex situ measurement might not have accurately reflected the actual concentrations of oxygen vacancies of selected samples under realistic reaction temperature (150–600°C). In our catalyst system, although the O_{ads}/O_{latt} values for the surface of all the four catalysts were close, more active oxygen species might be formed at the reaction temperature on the 0.5Pd/M-Co_1Ni_4 catalyst, as revealed by following H_2-TPR and O_2-TPD experiments, to contribute to an improvement of the performance (see Fig. 5).

According to published data, the binding energies of Pd $3d_{5/2}$ state (Fig. 4D) at 335.2–335.6, 336.5–337.7 and 338.0–338.7 eV represent Pd^0, PdO and Pd^{4+} species, respectively [3,37]. With specific regard to PdO component, well-crystalline PdO phase can be generally detected at 336.5 ± 0.2 eV, while peaks at higher binding energies (ca. 337.5 eV) correspond to highly dispersed Pd^{2+} species due to the final-state screening effects [31,38], since the localized d-electron cannot screen the hole generated by the photoemission effectively with the decrease of particle size. Therefore, the palladium species centered at binding energies of 337.6 and 338.7 eV in both 0.5Pd/Co_1Ni_4 and 0.5Pd/M-Co_1Ni_4 can be indexed separately into ultrafine PdO and Pd^{4+} species, in agreement with the XRD and HRTEM results. Furthermore, the analysis of Pd^{4+}/Pd^{2+} atomic ratio was also carried out using same method as that of Co 2p spectra, as compiled in Table 1. An observation of Pd^{4+}/Pd^{2+} and Co^{3+}/Co^{2+} ratios shows that 0.5Pd/M-Co_1Ni_4 has higher Pd^{4+}/Pd^{2+} ratio (0.59) but lower Co^{3+}/Co^{2+} value (0.62) than 0.5Pd/Co_1Ni_4 (see Table 1). Considering the powerful oxidation of trivalent cobalt cations, in present work, we tentatively deduce that

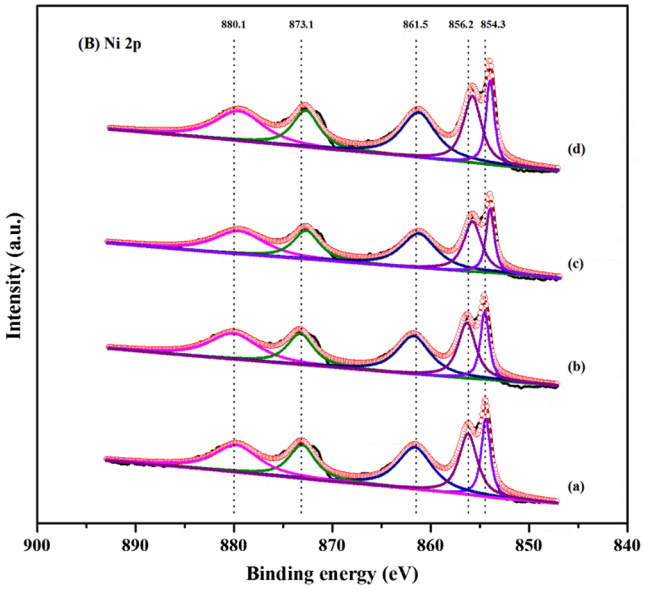

Fig. 4b. Ni 2p XPS spectra of (a) Co_1Ni_4, (b) M-Co_1Ni_4, (c) 0.5Pd/Co_1Ni_4 and (d) 0.5Pd/M-Co_1Ni_4.

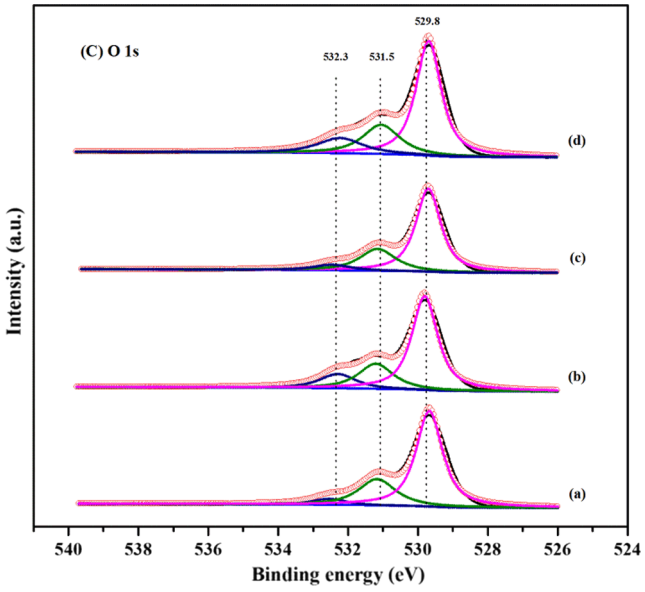

Fig. 4c. O 1s XPS spectra of (a) Co_1Ni_4, (b) M-Co_1Ni_4, (c) 0.5Pd/Co_1Ni_4 and (d) 0.5Pd/M-Co_1Ni_4.

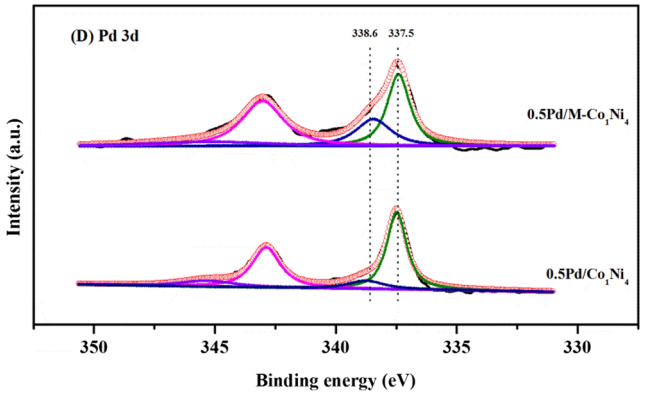

Fig. 4d. Pd 3d XPS spectra of 0.5Pd/Co_1Ni_4 and 0.5Pd/M-Co_1Ni_4.

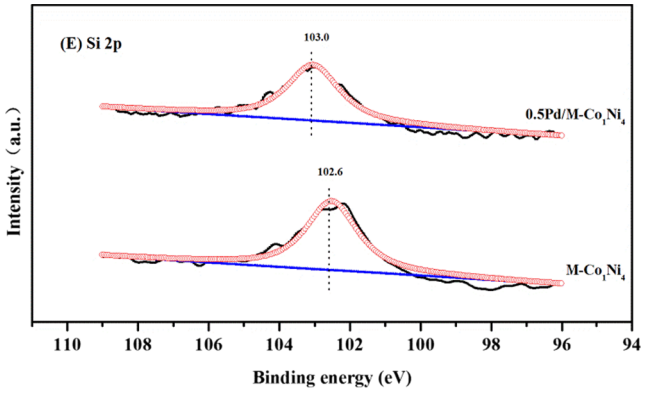

Fig. 4e. Si 2p XPS spectra of M-Co_1Ni_4 and 0.5Pd/M-Co_1Ni_4.

palladium species could be oxidized by Co^{3+} (i.e., electrons transferred from palladium to cobalt). Such a synergistic interaction could have given rise to the formation of Pd^{4+} species and further affected the light-off performance of 0.5Pd/Co_1Ni_4 and 0.5Pd/M-Co_1Ni_4. Indeed, It has been claimed that transient Pd^{4+} site could be stabilized in PdO_x clusters partially embedded in the CeO_2 lattice [7,8] or incorporated into the host matrix to form Pd-$LaFeO_3$ solid solution [3], and such sites could activate methane more efficiently than PdO (1 0 1) surface. Accordingly, in our Pd/Co_1Ni_4 system, one cannot exclude the presence of Pd^{4+} species doped into the lattice of NiO and/or $NiCo_2O_4$ taking the close ionic radius of Pd^{4+} (0.062 nm) [39], Ni^{2+} (0.069 nm) [17], Co^{2+} (0.072 nm) [40] and Co^{3+} (0.055 nm) [18] into consideration.

The effect of silicon, as an additional element in 0.5Pd/M-Co_1Ni_4 (different from 0.5Pd/Co_1Ni_4), on the physicochemical properties and catalytic performance would be very important. Consequently, the Si 2p spectra of M-Co_1Ni_4 and 0.5Pd/M-Co_1Ni_4 were fitted and shown in Fig. 4E. As in reported studies, peaks at binding energies of 98.8–99.7, 100.0–102.0 and 102.6–103.2 eV are contributed from Si^0, SiO_x ($0 < x < 2$) and SiO_2 [41,42], respectively. Therefore, our results unambiguously reveal that silicon species are present as SiO_2 in both samples, corroborating the hypothesis on the thermal evolution of reacted TEOOS mentioned above. In addition, the weight percentage of Si was also calculated based on XPS and listed in Table 1. Given the fact that XPS is a surface detection technique, these results were reasonable although they were slightly higher than the theoretical value (4.75 wt %) assuming that all the TEOOS molecules were reacted and then integrated to the surface of Co_1Ni_4 supports. However, corresponding peaks of M-Co_1Ni_4 and 0.5Pd/M-Co_1Ni_4 appear at 102.6 and 103.0 eV, respectively. Such a chemical shift implies that Si could modify the Pd-support interaction through electron transfer, thereby, enhancing the light-off activity of 0.5Pd/M-Co_1Ni_4.

Combined with associated performance shown below, one can tentatively conclude that the excellent performance of 0.5Pd/M-Co_1Ni_4 could have been a result of the synergistic interaction between Co_1Ni_4 support and PdO_x ($1 < x < 2$) phase, which was also modified by silicon species simultaneously.

3.4. Redox property and lattice oxygen activity

Fig. 5A demonstrates the H_2-TPR profiles of 0.5Pd/Co_1Ni_4 and 0.5Pd/M-Co_1Ni_4 in order to probe the redox behavior of these two samples. As can be seen, three successive peaks are observed in the H_2-TPR result of 0.5Pd/Co_1Ni_4. The weak peak located at 245℃ arises from Co^{3+} reduction to Co^{2+} [29,43], while the interpretation of the broader peak with maxima at the higher temperature region (ca. 350℃) is complicated by its poorly-resolved shoulder at approximately 300℃. From published data, both the reduction of NiO to metallic Ni and CoO to metallic Co generally occurs in the temperature range of 300–400℃ [18,30]. Thus their reduction peaks might have partially overlapped to

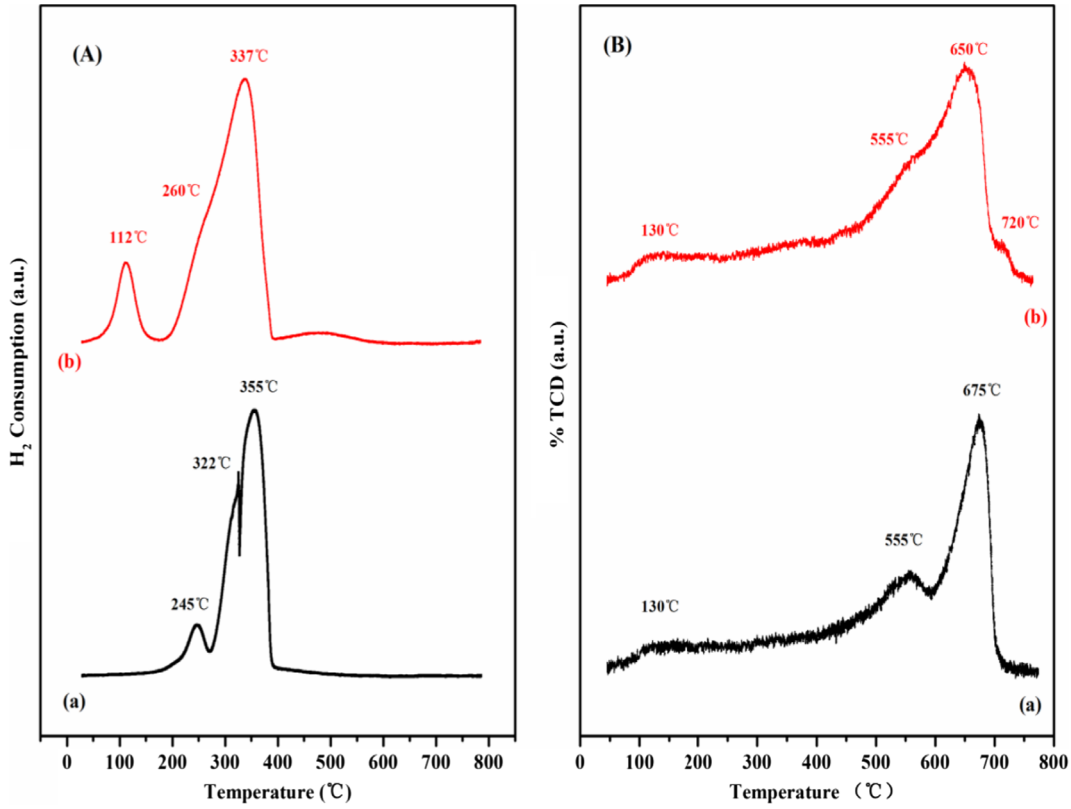

Fig. 5. (A) H_2-TPR and (B) O_2-TPD profiles of (a) 0.5Pd/Co_1Ni_4 and (b) 0.5Pd/M-Co_1Ni_4.

generate a broad peak, rationalizing the distinct shape of this curve. After the modification of Co_1Ni_4 support, 0.5Pd/M-Co_1Ni_4 exhibited a much better redox ability which does not only reflect in the shifts of reduction peaks towards lower temperatures but also in the larger H_2 consumption (14.3 mmol/g) than that of 0.5Pd/Co_1Ni_4 (13.4 mmol/g). Specifically, the three-step reduction process became almost indistinguishable in the H_2-TPR profile of 0.5Pd/M-Co_1Ni_4, which merged to form an intense and broad peak situated at 337℃ (about 20℃ lower than that of 0.5Pd/Co_1Ni_4) with a shoulder at 260℃, suggesting that the introduction of SiO_2 modification layer significantly affected the reduction of cobalt and nickel species. It is also worth noting that a new reduction peak appears at 112℃, a temperature at which only noble metal could be reduced by H_2 [3,44]. Nevertheless, the corresponding H_2 consumption of this peak is calculated to be 1447 μmol/g, which is much higher than the stoichiometric amount of H_2 needed for the reduction of PdO to Pd (47 μmol/g), and more than that required for the conversion of PdO_2 to Pd (94 μmol/g) assuming a theoretical Pd loading of 0.5 wt%. Meanwhile, because of the irreducible nature of SiO_2 [45], the lattice oxygen of SiO_2 cannot be reduced at this temperature as well. Hence, one can safely ascribe this low temperature reduction peak to the depletion of reactive oxygen species [18,46], which could be adsorbed and activated on vacant oxygen sites and participate in the subsequent oxidation reaction of methane. Such an improvement on reducibility is closely associated with the formation of oxygen vacancies and believed to have positive impact on the oxidation of hydrocarbons according to the MvK mechanism, explaining the enhanced activity of 0.5Pd/M-Co_1Ni_4.

O_2-TPD experiments were also conducted to gain insight into the composition and mobility of oxygen species, as shown in Fig. 5B. Generally, transition metal oxide based catalysts present three kinds of oxygen in different temperature ranges. One is the molecular oxygen species adsorbed on the catalyst surface (O_2^-) which generally account for desorption peaks in the temperature region below 400℃. Oxygen molecules released from sub-surface lattice oxygen which are in the intermediate temperature range of 400 to 600℃, constitute another kind. The third is the bulk lattice oxygen O^{2-} species which give peaks in the temperature region exceeding 600℃ [47]. By checking the O_2-TPD results of 0.5Pd/Co_1Ni_4, the weak but broad desorption peak extending from 50 to 400℃ is attributed to the liberation of molecular O_2^-, while the well-defined peaks with maxima at 555 and 675℃ belong to the oxygen stripped from subsurface and bulk lattice of Co_1Ni_4 carrier, respectively. For the sample of 0.5Pd/M-Co_1Ni_4, the desorption peaks of corresponding oxygen species are found at 130, 555 and 650℃, accompanied by the appearance of an additional peak situated at 720℃ which belongs to the O_2 released from palladium oxide (PdO and PdO_2) [37,48,49]. The desorption behavior of surface adsorbed oxygen components in low temperature region shows no obvious difference between these two samples. However, in the result of 0.5Pd/M-Co_1Ni_4, the intensity of desorption peak in the temperature range of 555 to 650℃ is stronger than that of 0.5Pd/Co_1Ni_4, demonstrating that the 0.5Pd/M-Co_1Ni_4 could supply much more sufficient oxygen species during reaction process than 0.5Pd/Co_1Ni_4. Furthermore, there are no signals associated with palladium in the TPD curve of 0.5Pd/Co_1Ni_4. Combined with the different electronic properties of supported palladium species determined by XPS, we deduced that the presence of SiO_2 might have weakened the bond strengthen of Pd-O and facilitated the desorption of oxygen in the 0.5Pd/M-Co_1Ni_4 catalyst [50], while the Pd-O bond in 0.5Pd/Co_1Ni_4 was too stable to crack even at elevated temperature, providing a plausible explanation for the absence of desorption peak ascribable to palladium oxide.

3.5. Catalytic performance and thermal stability test

Fig. 6 compares the light-off performance of samples tested in the temperature region of 150 to 600℃, while Table 2 summarizes their exact temperatures at which the methane conversion reached 10%, 50% and 90% (T_{10}, T_{50} and T_{90}). A completed screening of Pd loadings (0.25, 0.5, 1.0, and 2.0 wt%) has revealed that the optimum Pd content

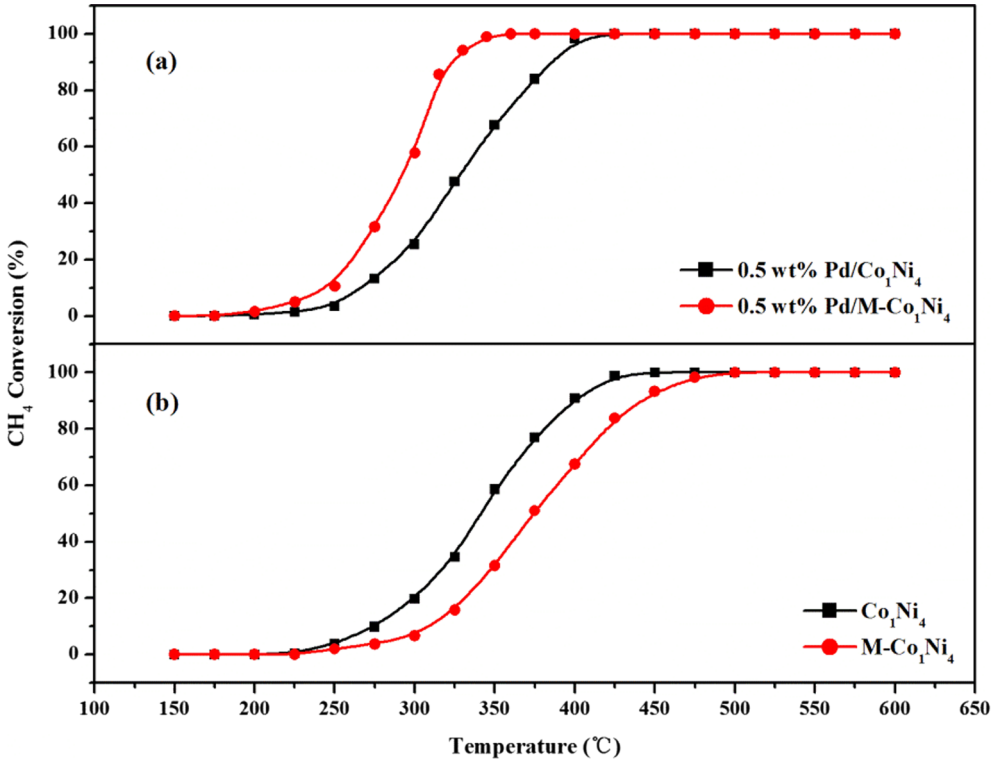

Fig. 6. Methane conversion as a function of temperature over (a) 0.5Pd/Co_1Ni_4, 0.5Pd/M-Co_1Ni_4 and (b) Co_1Ni_4, M-Co_1Ni_4. Reaction conditions: catalyst quantity = 20 mg, GHSV = 60,000 $mLg^{-1}h^{-1}$, feed steam consisted of 1 vol% CH_4 and 99 vol% air.

Table 2
Catalytic performance of tested samples.

Catalyst	T_{10} [℃]	T_{50} [℃]	T_{90} [℃]	Specific reaction rate[a] [μmol/(g_{cat}·s)]
Co_1Ni_4	274	341	402	0.43
M-Co_1Ni_4	308	374	442	0.18
0.5Pd/Co_1Ni_4	266	328	385	0.55
0.5Pd/M-Co_1Ni_4	243	292	323	1.36

a. Methane combustion at 260℃.

is 0.5 wt% under our experimental conditions, so we chose this loading content and further investigated the effect of our strategy on the performance.

As shown in Fig. 6 and Table 2, bare Co_1Ni_4 binary oxide was intrinsically active for the oxidation of CH_4, exhibiting a T_{90} temperature of 402℃. The introduction of silicon species resulted in a slight reduction in the activity of M-Co_1Ni_4 (T_{90} = 385℃), which might be relevant to the coverage of active sites of inert SiO_2. With the loading of palladium phases, 0.5Pd/Co_1Ni_4 did not show a significant improvement on light-off activity compared to pure Co_1Ni_4. However, it is important to note that 0.5Pd/M-Co_1Ni_4 possessed a much better activity than the other three samples, having achieved 90% methane conversion at 323℃. To evaluate the inherent catalytic activity more accurately, the specific reaction rate at a desired temperature (260℃) of the four samples were also calculated and shown in Table 2. Clearly, 0.5Pd/M-Co_1Ni_4 gave the highest value of 1.36 μmol/(g_{cat}·s), and the reaction rates in increasing sequence is as follows: M-Co_1Ni_4 < Co_1Ni_4 < 0.5Pd/Co_1Ni_4 < 0.5Pd/M-Co_1Ni_4.

Overall, our test results demonstrated that the presence of silicon phase effectively improved the utilization of Co_1Ni_4 carrier and active palladium phase, while the combination of Co_1Ni_4 mixed oxide and Pd (or Si) alone did not achieve high catalytic efficiency towards methane combustion. Over the last ten years, a considerable number of supported palladium catalysts have been developed for CCM, and their performance in terms of T_{50} and T_{90} are summarized in Table 3. In spite of the relatively lower loading of noble metal (0.5 wt%) and higher space velocity (60,000 $mLg^{-1}h^{-1}$), 0.5Pd/M-Co_1Ni_4 gave a performance close to that of 2.94$Au_{0.5}$Pd/meso-Co_3O_4 [28], which was better than those of 2.0Pd/$LaFeO_3$ [3], 3.0Pd/Co_3O_4 [26], 2.0Pd/o-CeO_2 [6], 0.5Pd/κ-CZ [25], etc.

Besides low-temperature activity, thermal stability is another

Table 3
A literature review of methane combustion activity over supported Pd catalysts in terms of T_{50} and T_{90}.

Catalyst	Concentration of CH_4 [vol%]	GHSV [$mLg^{-1}h^{-1}$]	T_{50} [℃]	T_{90} [℃]	Content of noble metal [wt%]	Reference
Pd/$LaFeO_3$	1.0	18,400	460	600	2.0	[3]
Pd@CeO_2/H-Al_2O_3	0.5	200,000	320	370	1.0	[23]
Pd/$LaMnO_3$	1.0	20,000	425	500	1.5	[51]
AuPd/meso-Co_3O_4	2.5	20,000	280	324	3.0	[28]
Au Pd/3DOM LSMO	5.0	50,000	314	336	3.0	[52]
Pd/Co_3O_4	2.0	12,000	333	~370	3.0	[26]
Pd/o-CeO_2	1.0	30,000	309	348	2.0	[6]
Pd/m-zeolite	1.0	69,000	355	375	0.5	[53]
Pd/κ-CZ	1.0	30,000	~305	345	0.5	[25]
Pd/M-Co_1Ni_4	1.0	60,000	292	323	0.5	Present work

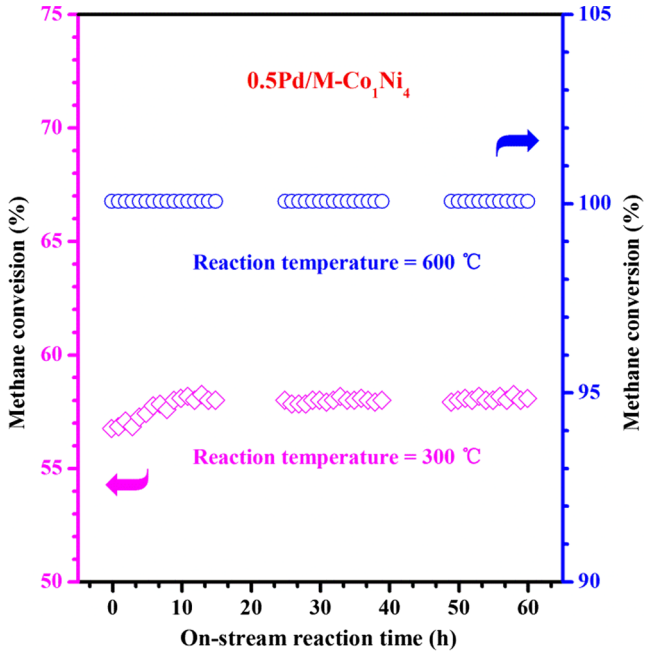

Fig. 7. On-stream reaction of 0.5Pd/M-Co_1Ni_4 at 300°C and 600°C.

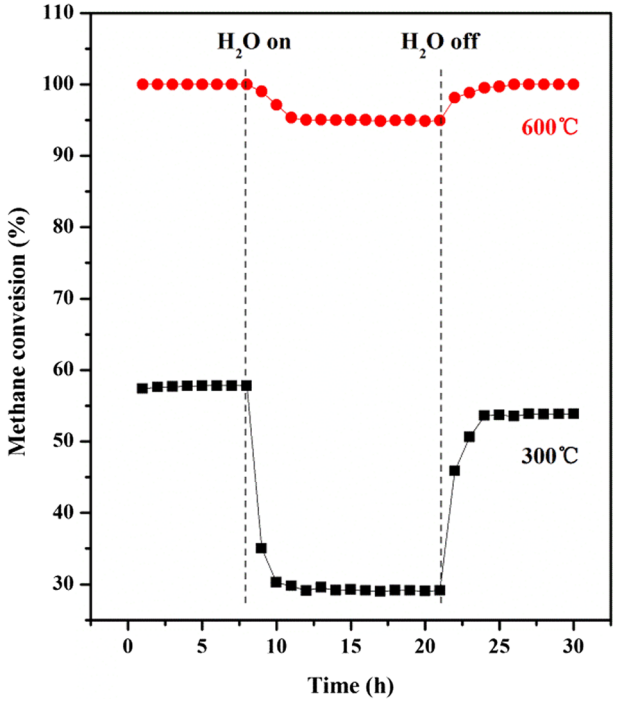

Fig. 8. Effect of water introduction and cutting off in the feedstock over 0.5Pd/M-Co_1Ni_4 at 300°C and 600°C (H_2O concentration 5.0 vol%).

important index when evaluating methane combustion catalysts. Therefore, the on-stream methane oxidation over our best-performing 0.5Pd/M-Co_1Ni_4 catalyst was conducted at temperatures of 300°C and 600°C, as shown in Fig. 7. Although it has been reported that $NiCo_2O_4$ would decompose to NiO above 400°C [19], 100% methane conversion was maintained within 60 h during the on-stream reaction at 600°C, illustrating an excellent stability of 0.5Pd/M-Co_1Ni_4 under elevated temperature. Interestingly, one could also observe that the conversion of methane increased slightly in the first 10 h during the isothermal continuous experiment at 300°C, a result possibly due to the restruction and in situ formation of active sites under the reaction condition. Experiments in which the hydrothermal stability of 0.5Pd/M-Co_1Ni_4 was examined through 30 h on steam methane combustion in the presence of 5.0 vol% water were also completed, as shown in Fig. 8. The water-resistance capability of 0.5Pd/M-Co_1Ni_4 was low at 300°C, over which the conversion of methane reduced from 58% to 29%, proving that the amorphous SiO_2 might be poor in hydrothermal stability. When the water vapor was cut off, the CH_4 conversion gradually restored to 54%, which was still lower than its initial value in the absence of water. As the temperature rose to 600°C, the addition of 5.0 vol% water vapor cannot significantly affect the catalytic activity of 0.5Pd/M-Co_1Ni_4 anymore, only slight deterioration was observed and the conversion could recover completely after the removal of water.

4. Conclusion

In this work, ultrafine palladium nanoparticles were supported on surface-modified Co_1Ni_4 oxide and employed as a high-performance CCM catalyst. Through a simple reflux process, the alkyl chains of TEOOS successfully attached on the surface of Co_1Ni_4 support and eventually evolved into amorphous SiO_2 phase, as confirmed by HRTEM, transmission FTIR and Si 2p XPS spectra. Catalytic tests on lean methane oxidation revealed that such a surface modification strategy significantly promoted the low-temperature performance of 0.5Pd/M-Co_1Ni_4, over which the temperature required for 90% methane conversion was 323°C, while providing excellent thermal stability at 600°C. The physicochemical properties of selected samples were further substantiated through various characterization techniques. The results revealed that the support modification effectively altered the interaction between palladium and Co_1Ni_4 support, as reflected by the higher Pd^{4+}/Pd^{2+} but lower Co^{3+}/Co^{2+} ratios in 0.5Pd/M-Co_1Ni_4 when compared to 0.5Pd/Co_1Ni_4. Moreover, combined with the analysis of H_2-TPR and O_2-TPD profiles, it can be deduced that the introduced silicon species improved the low temperature reducibility and the amount of reactive adsorbed oxygen as well, which helped in the supply of abundant oxygen species during the oxidation reaction. All these factors contributed to the enhanced performance of 0.5Pd/M-Co_1Ni_4 catalyst in the lean methane combustion.

Author contributions

Cunshuo Li, Wenzhi Li and Qiuyan Duan: Conceptualization and Methodology; **Cunshuo Li:** Writing - original draft; **Wenzhi Li, Ajibola T. ogunbiyi and Zean Zhou:** Writing - review & editing; **Wenzhi Li:** Funding acquisition; **Cunshuo Li and Fengyang Xue:** Investigation.

Declaration of Competing Interest

The authors declare that they have no known competing financial interests or personal relationships that could have appeared to influence the work reported in this paper.

Acknowledgment

This work was supported by the Program of National Natural Science Foundation of China (51676178), the Fundamental Research Funds for the Central Universities (WK2090130026).

Appendix A. Supplementary data

Supplementary data to this article can be found online at https://doi.org/10.1016/j.fuel.2020.118372.

References

[1] Li W, Liu D, Feng X, Zhang Z, Jin X, Zhang Y. High-performance ultrathin Co_3O_4 nanosheet supported PdO/CeO_2 catalysts for methane combustion. Adv Energy

Mater 2019;9(18):1803583.
[2] Stakheev AY, Batkin AM, Teleguina NS, Bragina GO, Zaikovsky VI, Prosvirin IP, et al. Particle size effect on CH_4 oxidation over noble metals: comparison of Pt and Pd catalysts. Top Catal 2013;56:306–10.
[3] Eyssler A, Winkler A, Mandaliev P, Hug P, Weidenkaff A, Ferri D. Influence of thermally induced structural changes of 2 wt% Pd/$LaFeO_3$ on methane combustion activity. Appl Catal B 2011;106(3–4):494–502.
[4] Dai Y, Kumar VP, Zhu C, Wang H, Smith KJ, Wolf MO, et al. Bowtie-shaped $NiCo_2O_4$ catalysts for low-temperature methane combustion. Adv Funct Mater 2019;29(8):1807519.
[5] Zhang Z, Li J, Yi T, Sun L, Zhang Y, Hu X, et al. Surface density of synthetically tuned spinel oxides of Co^{3+} and Ni^{3+} with enhanced catalytic activity for methane oxidation. Chin J Catal 2018;39(7):1228–39.
[6] Lei Y, Li W, Liu Q, Lin Q, Zheng X, Huang Q, et al. Typical crystal face effects of different morphology ceria on the activity of Pd/CeO_2 catalysts for lean methane combustion. Fuel 2018;233:10–20.
[7] Senftle TP, van Duin ACT, Janik MJ. Methane Activation at the Pd/CeO_2 Interface. ACS Catal 2016;7(1):327–32.
[8] Senftle TP, van Duin ACT, Janik MJ. Role of site stability in methane activation on $Pd_xCe_{1-x}o_8$ surfaces. ACS Catal 2015;5(10):6187–99.
[9] Baylet A, Royer S, Marécot P, Tatibouët JM, Duprez D. High catalytic activity and stability of Pd doped hexaaluminate catalysts for the CH_4 catalytic combustion. Appl Catal B 2008;77(3–4):237–47.
[10] Liu Y, Wang S, Gao D, Sun T, Zhang C, Wang S. Influence of metal oxides on the performance of Pd/Al_2O_3 catalysts for methane combustion under lean-fuel conditions. Fuel Process Technol 2013;111:55–61.
[11] Takeguchi T. Strong chemical interaction between PdO and SnO_2 and the influence on catalytic combustion of methane. Appl Catal A 2003;252(1):205–14.
[12] Takeguchi T, Aoyama S, Ueda J, Kikuchi R, Eguchi K. Catalytic combustion of volatile organic compounds on supported precious metal catalysts. Top Catal 2003;23:159–62.
[13] Yin F, Ji S, Wu P, Zhao F, Li C. Deactivation behavior of Pd-based SBA-15 mesoporous silica catalysts for the catalytic combustion of methane. J Catal 2008;257(1):108–16.
[14] Gholami R, Smith KJ. Activity of PdO/SiO_2 catalysts for CH_4 oxidation following thermal treatments. Appl Catal B 2015;168–169:156–63.
[15] Guerrero S, Araya P, Wolf E. Methane oxidation on Pd supported on high area zirconia catalysts. Appl Catal A 2006;298:243–53.
[16] Park J-H, Cho JH, Kim YJ, Kim ES, Han HS, Shin C-H. Hydrothermal stability of Pd/ZrO_2 catalysts for high temperature methane combustion. Appl Catal B 2014;160–161:135–43.
[17] Zhang Y, Qin Z, Wang G, Zhu H, Dong M, Li S, et al. Catalytic performance of MnO_x-NiO composite oxide in lean methane combustion at low temperature. Appl Catal B 2013;129:172–81.
[18] Chen J, Zhang X, Arandiyan H, Peng Y, Chang H, Li J. Low temperature complete combustion of methane over cobalt chromium oxides catalysts. Catal Today 2013;201:12–8.
[19] Shao C, Li W, Lin Q, Huang Q, Pi D. Low temperature complete combustion of lean methane over cobalt-nickel mixed-oxide catalysts. Energy Technol 2017;5(4):604–10.
[20] Tao FF, Shan JJ, Nguyen L, Wang Z, Zhang S, Zhang L, et al. Understanding complete oxidation of methane on spinel oxides at a molecular level. Nat Commun 2015;6:7798.
[21] Li J, Liang X, Xu S, Hao J. Catalytic performance of manganese cobalt oxides on methane combustion at low temperature. Appl Catal B 2009;90(1–2):307–12.
[22] Machej T, Serwicka EM, Zimowska M, Dula R, Michalik-Zym A, Napruszewska B, et al. Cu/Mn-based mixed oxides derived from hydrotalcite-like precursors as catalysts for methane combustion. Appl Catal A 2014;474:87–94.
[23] Cargnello M, Jaén JJD, Garrido JCH, Bakhmutsky K, Montini T, Gámez JJC, et al. Exceptional activity for methane combustion over modular Pd@CeO_2 subunits on functionalized Al_2O_3. Science 2012;337:713–7.
[24] Duan Q, Zhang C, Sun S, Pan Y, Zhou X, Liu Y, et al. Atomically dispersed palladium-based catalysts obtained via constructing a spatial structure with high performance for lean methane combustion. J Mater Chem A 2020;8:7395–404.
[25] Ding Y, Wu Q, Lin B, Guo Y, Guo Y, Wang Y, et al. Superior catalytic activity of a Pd catalyst in methane combustion by fine-tuning the phase of ceria-zirconia support. Appl Catal B 2020;266:118631.
[26] Ercolino G, Stelmachowski P, Grzybek G, Kotarba A, Specchia S. Optimization of Pd catalysts supported on Co_3O_4 for low-temperature lean combustion of residual methane. Appl Catal B 2017;206:712–25.
[27] Sun Y, Liu J, Yang N, Zhu Y. One-dimensional heterostructured palladium oxide-cobalt oxide catalyst for the catalytic oxidation of methane. ChemCatChem 2017;9(5):738–45.
[28] Wu Z, Deng J, Liu Y, Xie S, Jiang Y, Zhao X, et al. Three-dimensionally ordered mesoporous Co_3O_4-supported Au–Pd alloy nanoparticles: high-performance catalysts for methane combustion. J Catal 2015;332:13–24.
[29] Gou Y, Liang X, Chen B. Porous Ni–Co bimetal oxides nanosheets and catalytic properties for CO oxidation. J Alloy Compd 2013;574:181–7.
[30] Lim TH, Cho SJ, Yang HS, Engelhard MH, Kim DH. Effect of Co/Ni ratios in cobalt nickel mixed oxide catalysts on methane combustion. Appl Catal A 2015;505:62–9.
[31] Wang C, Wen C, Lauterbach J, Sasmaz E. Superior oxygen transfer ability of Pd/MnO_x-CeO_2 for enhanced low temperature CO oxidation activity. Appl Catal B 2017;206:1–8.
[32] Zhu Huaqing, Qin Zhangfeng, Shan Wenjuan, Shen Wenjie, Wang J. Pd/CeO_2–TiO_2 catalyst for CO oxidation at low temperature a TPR study with H_2 and CO as reducing agents. J Catal 2004;225:267–77.
[33] Wang H, Tang M, Zhang K, Cai D, Huang W, Chen R, et al. Functionalized hollow siliceous spheres for VOCs removal with high efficiency and stability. J Hazard Mater 2014;268:115–23.
[34] Agrawal S, Parveen A, Azam A. Microwave assisted synthesis of Co doped NiO nanoparticles and its fluorescence properties. J Lumin 2017;184:250–5.
[35] Davar F, Fereshteh Z, Salavati-Niasari M. Nanoparticles Ni and NiO: synthesis, characterization and magnetic properties. J Alloy Compd 2009;476(1–2):797–801.
[36] Arandiyan H, Dai H, Ji K, Sun H, Li J. Pt nanoparticles embedded in colloidal crystal template derived 3D ordered macroporous $Ce_{0.}$ $6Z_{r0.}3_{Y0.}1_O2$: highly efficient catalysts for methane combustion. ACS Catal 2015;5(3):1781–93.
[37] Persson K, Ersson A, Fierro JLG, Järås SG, Influence of molar ratio on Pd–Pt catalysts for methane combustion. J Catal 2006, 243, 14–24.
[38] Penner S, Bera P, Pedersen S, Ngo LT, Harris JJW, Campbell CT. Interactions of O_2 with Pd nanoparticles on r-Al_2O_3(0001) at low and high O_2 pressures. J Phys Chem B 2006;110:24577–84.
[39] Nishihata Y, Mizuki J, Akao T, Tanaka H, Uenishi M, Kimura M, et al. Self-regeneration of a Pd-perovskite catalyst for automotive emissions control. Nature 2002;418:164–7.
[40] Li W, Wang G, Chen C, Liao J, Li Z. Enhanced Visible Light Photocatalytic Activity of ZnO Nanowires Doped with Mn^{2+} and Co^{2+} Ions. Nanomaterials 2017;7:(1).
[41] Barr TL. An XPS study of Si as it occurs in adsorbents, catalysts. Applications Surface Sci 1983, 15, 1-35.
[42] Chenakin SP, Melaet G, Szukiewicz R, Kruse N. XPS study of the surface chemical state of a Pd/(SiO_2 + TiO_2) catalyst after methane oxidation and SO_2 treatment. J Catal 2014;312:1–11.
[43] Ren Z, Wu Z, Song W, Xiao W, Guo Y, Ding J, et al. Low temperature propane oxidation over Co_3O_4 based nano-array catalysts: Ni dopant effect, reaction mechanism and structural stability. Appl Catal B 2016;180:150–60.
[44] Dutov VV, Mamontov GV, Zaikovskii VI, Liotta LF, Vodyankina OV. Low-temperature CO oxidation over Ag/SiO_2 catalysts: Effect of OH/Ag ratio. Appl Catal B 2018;221:598–609.
[45] Zhu Y, Kong X, Yin J, You R, Zhang B, Zheng H, et al. Covalent-bonding to irreducible SiO_2 leads to high-loading and atomically dispersed metal catalysts. J Catal 2017;353:315–24.
[46] Zhang W, Wu F, Li J, You Z. Dispersion–precipitation synthesis of highly active nanosized Co_3O_4 for catalytic oxidation of carbon monoxide and propane. Appl Surf Sci 2017;411:136–43.
[47] Liu F, Rong S, Zhang P, Gao L. One-step synthesis of nanocarbon-decorated MnO_2 with superior activity for indoor formaldehyde removal at room temperature. Appl Catal B 2018;235:158–67.
[48] Zhao X, Liu Y, Deng J, Xu P, Yang J, Zhang K, et al. Mesoporous Pd_xPt alloys: High-performance catalysts for methane combustion. Molecular Catalysis 2017;442:191–201.
[49] Widjaj H, Sekizaw K, Eguchi K, Arai H. Oxidation of methane over Pd/mixed oxides for catalytic combustion. Catal Today 1999;47:95–101.
[50] Wang C-B, Ho C-M, Lin H-K, Chiu H-C. Low temperature complete combustion of methane over titania-modified alumina-supported palladium. Fuel 2002;81:1883–7.
[51] Guo G, Lian K, Gu F, Han D, Wang Z. Three dimensionally ordered macroporous Pd-$LaMnO_3$ self-regeneration catalysts for methane combustion. Chem Commun 2014;50(88):13575.
[52] Wang Y, Arandiyan H, Scott J, Akia M, Dai H, Deng J, Kondo-Francois, Aguey-Zinsou, Amal R. High performance Au–Pd supported on 3D hybrid strontium-substituted lanthanum manganite perovskite catalyst for methane combustion. ACS Catal 2016;6:6935–47.
[53] Losch P, Huang W, Vozniuk O, Goodman ED, Schmidt W, Cargnello M. Modular Pd/zeolite composites demonstrating the key role of support hydrophobic/hydrophilic character in methane catalytic combustion. ACS Catal 2019;9:4742–53.